ISABE-2011-1721

INTEGRATED DESIGN OF ROTOR LEADING EDGE AND CAVITY FLOWS IN AN AXIAL SHROUDED TURBINE

Konstantinos G. Barmpalias, Reza S. Abhari
Laboratory for Energy Conversion
Department of Mechanical and Process Engineering
ETH Zurich
Zurich, Switzerland

Anestis I. Kalfas
Laboratory of Fluid Mechanics and Turbomachinery
Department of Mechanical Engineering
Aristotle University of Thessaloniki
Greece

Naoki Shibukawa
Kehin Product Operations, Toshiba Corporation
Power and Industrial Systems R & D Center, Toshiba Corporation

Takashi Sasaki
Thermal and Hydro Power Systems and Services Division
Toshiba Corporation, 105-8001
Tokyo, Japan

Abstract

In this paper we examine the impact of rotor leading edge modifications on stage efficiency through their influence on the flow field and their interaction with the cavity flows. Three rotor leading edge modifications have been examined. The interaction of the cavity and main flows results in a false incidence on the rotor blade. The re-entry of part of the leakage flow back into the mainstream heavily impacts the main flow path, thus generating a false incidence on the downstream bladerow for the span locations above 75%. The initial leading edge metal angle of -19°(compared to the axial direction) was modified to +12° to better match the flow field as this was experimentally measured and computationally predicted. An efficiency gain of 0.21% was attributed to loss minimization due to the corrected incidence. Nevertheless, a modification of the metal angle to -30° met with success, increasing the efficiency by 0.19%. A supplementary computational analysis revealed that the lean imposed on the blade caused the tip passage vortex to lose strength and migrate to a lower span location.

Nomenclature

C_z	axial chord length
D	probe head diameter
h	non-dimensional blade span
P	pressure
P_{max}	maximum pressure
r	radial direction
S	non-dimensional streamwise distance
y^+	dimensionless wall distance
z	axial direction
Z	non-dimensional stator rotor distance
θ	circumferential direction
σ	solidity

Subscripts

z	axial direction
max	maximum

Abbreviations

CFD	computational fluid dynamics
EXP	experimental
LS	low solidity

Introduction

Losses due to changes in incidence angle at the tip section of the blade due to prior mixing of the cavity and main flows account for a substantial part of the total aerodynamic losses in shrouded turbines. After having been circulated inside the rotor inlet cavity by the toroidal vortex, part of the leakage flow that is driven by the pressure difference across the rotor through the labyrinth re-enters the main flow causing extensive mixing in the interaction zone[1]. The difference in flow angle between the re-injected cavity flow and the main flow is what facilitates the false incidence on the downstream bladerow. Wallis et al.[2] and Rosic and Denton[3] attempted to guide the cavity flow back into the main flow with the use of bladelets positioned on the shroud and on the stationary cavity wall, respectively. Only Rosic and Denton[3] manage to successfully lead the cavity flow with a corrected flow angle back into the main flow and were able to report an efficiency increase of 0.4%. Using a similar approach, Mahle[4] reported marginal efficiency gains in a computational study. Peters et al.[5], Anker et al.[6] and Gier et al.[7] reported on the strong interactions between cavity and main flow and examined the different loss-generating mechanics. They discussed the secondary channel vortex and its strengthening due to the egress of the cavity flow. On the same topic, Pau et al.[8] studied the impact of the leakage flow on the main flow. They showed that there is an enhancement of all counter-rotating vortices with respect to the main passage vortex due to the low turning that is experienced by the leakage flow. The strong negatively signed vorticity that dominates the secondary flows at the interaction zone has also been reported by Adami et al.[9]. Gregory-Smith et al.[10] successfully introduced the use of endwall profiling procedures to modify the secondary flow. Sauer et al.[11] proposed the use of leading edge modifications at the tip region to decrease secondary losses. Brenner et al.[12], Becz et al.[13] and Perdichizzi and Dossena[14] studied the influence of the leading edge geometry on secondary and endwall losses respectively. These studies have shown effectiveness in controlling secondary flow under controlled inflow conditions. Nevertheless, the inflow conditions are highly unsteady and three-dimensional[15-16]. Blade row interactions[17-18] wake-blade and vortex-blade interactions[19-20], as well as the presence of open cavities[21], all contribute to the unsteadiness of the flow field. Pfau et al.[22] systematically investigated cavity flows in different cavity configurations. They described in detail the toroidal vortex as the dominant kinematic flow feature in the cavity region. This vortex is fed with high-pressure fluid from the pressure side of the stator blade. The associated fluctuating mass in turn results in negative incidence on the rotor. Based on the secondary flow development and mixing losses they were able to make some design recommendations. A lot of work has been dedicated to the mixing occurring at the interaction between the cavity and main flows at the rotor exit cavity and its consequence on the downstream bladerow. On the other hand, the interaction between the two flows at the rotor inlet cavity that leads to a false incidence on the tip section of the rotor blade has not received much attention. In the present work this is examined in an experimental study of a baseline case and also verified by computational work and two additional cases that were computationally studied. The baseline case suffered from positive incidence. As a first step the rotor leading edge was varied to match the flow conditions that were experimentally measured and

computationally verified, leading to an efficiency increase. In a second approach the rotor leading edge was modified to create a more negative incidence. Nevertheless, an efficiency increase was again measured.

Rotor leading edge modification

Three different leading edge geometries of the second rotor were tested in this study. The baseline case and the two modifications are illustrated in Figure 1. The first modification has a positive metal angle (Figure 1a) and the second a more negative angle (Figure 1b) compared to the baseline case. The first modification has a positive metal angle to better match the positive incidence measured at the baseline case. To the contrary, the second modification received an even more negative metal angle. The profile of the blades was modified in the upper 30% of the blade height. Care was taken not to create a point of inflexion on both sides of the blades. Moreover, the center of pressure was kept constant for all three cases examined. From this point on, the modification with the positive metal angle will be referred to as Design A and the modification with the negative metal angle as Design B.

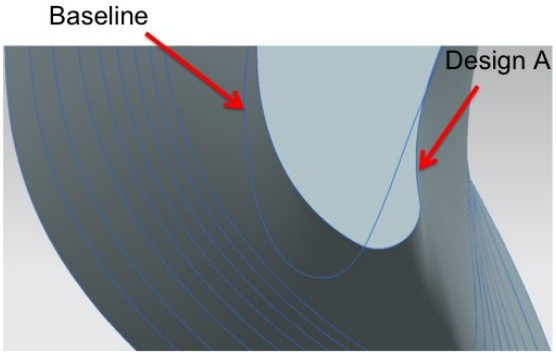

a.

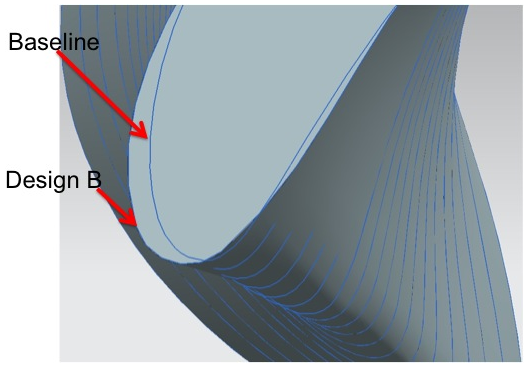

b.

Figure 1: Modifications of the rotor leading edge (a) positive metal angle, +12° and (b) negative metal angle, -30°. The baseline metal angle is at -19° . Data are taken from 100% of the blade span.

Experimental method

The research facility

The measurements were performed in the 'LISA' two-stage axial research turbine at the Laboratory for Energy Conversion (LEC) of ETH Zurich. The turbine inlet temperature, TET is kept constant at 310 K, with an accuracy of 0.9 K. A DC generator maintains a constant operating speed of 2750 ±0.5 RPM (±0.02%). The measurement uncertainty of the test facility concerning total-to-static efficiency of the second stage is ±0.21%. A more detailed description of the test facility is available in Schlienger et al.[23]. The stator blade row configurations differ, as shown in Table 1. The first stator is of a high solidity ($\sigma = 1.43$) design, whereas the second stator has low solidity ($\sigma = 1.25$). Both stators are designed to have the same exit flow angle and axial chord. The associated operating parameters based on the LS stator are summarized in Table 2. More detailed measurements on the baseline test case can be found in Tashima et al.[24].

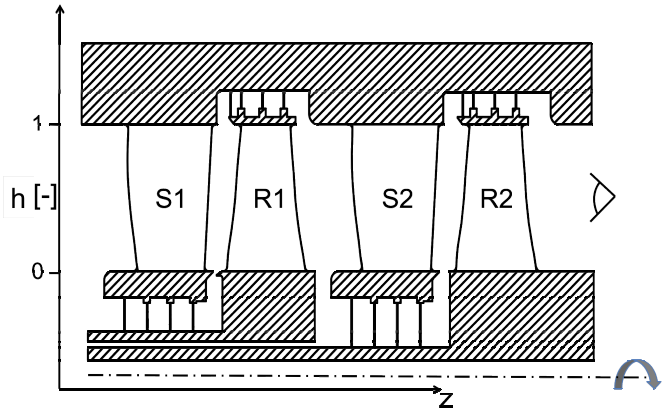

Figure 2: Schematic diagram of the two-stage axial turbine.

Parameter	HS stator	LS stator
Blade count Zs	48	36
Axial chord* C_z [mm]	50	50
Chord length* C [mm]	66.3	77.4
Pitch* T [mm]	46.5	62.0
Blade span H [mm]	90	90
Aspect ratio AR = H/C [-]	1.36	1.16
Solidity σ = C/T [-]	1.43	1.25

Table 1: Geometric details of stator blades. (* Indicates that the dimension is measured at 50% span)

Instrumentation

Both steady and unsteady flow field measurements are made. In the main flow the steady flow field is measured using a 5-hole pneumatic probe (5HP) with a 0.9 mm head diameter, whereas the unsteady flow field is captured with the use of a 2-sensor Fast Response Aerodynamic Probe (FRAP), which has a 1.8 mm head diameter, as shown in Figure 3. For the measurements inside the cavity, a miniature 4-hole pneumatic probe (4HP) was used for the steady flowfield together with a pair of miniature FRAP probes of 0.84mm head diameter for the unsteady flowfield.

Rotor speed [RPM]	2750
Overall pressure ratio [-]	1.32
Mass flow [kg/sec]	7.87
Turbine inlet temperature [°C]	37.8
Blade number count stage-1 (stator/rotor)	48/48
Blade number count stage-2 (stator/rotor)	36/48
Tip/hub diameter [mm]	800/620
Flow coefficient (stage-2) [-]	0.3
Loading coefficient (stage-2) [-]	1.0
Mach number (stator/rotor)	0.32/0.1
Reynolds number (rotor)	2×10^5

Table 2. Main parameters of the test case configuration based on the characteristics of the LS stator.

Each miniature FRAP probe is one-holed; one miniature FRAP is yaw sensitive and the other is used for the pitch measurement. A detailed description of the two miniature probes can be found in Pfau et al.[25] The FRAP has a measurement bandwidth of 48 kHz. The measured flow parameters and their absolute uncertainties are listed in Table 3. Absolute uncertainties of the measured flow quantities in Table 3 are expressed as a percentage of the calibration range for the angles, a percentage of the dynamic head for pressures and a percentage of the absolute Mach number for the velocity. The use of FRAP and pneumatic probes in the 'LISA' turbine facility has been detailed in several publications, including Lenherr et al.[26].

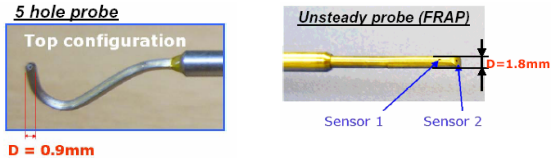

Figure 3: 5HP and 2-sensor FRAP measurement probes.

	α	γ	P_t	P_s	M
FRAP	0.5°	0.7°	1%	1.2%	1%
5HP	0.3°	0.3°	1.8%	2%	0.06%

Table 3: Absolute uncertainties in probe measurements for a calibration range of yaw ±30° pitch ±20° and for a Mach number of 0.3. (uncertainties in pressure are shown as a percentage of dynamic head, uncertainties in Mach number are shown as a percentage of the absolute Mach number).

Probe measurements were made at the rotor exit and downstream of the LS stator. Measurements at the stator exit were made 6mm downstream of the stator at h=1 while inside the cavity. The measurement plane is located at $0.224C_z$ downstream of the 2nd stator's trailing edge at midspan. The measurement grids consist of 48 points and 61 points evenly distributed in the radial and circumferential directions. The circumferential traverse was conducted over three LS stator pitches. Data are sampled at 200 kHz, which corresponds to 92 samples per blade passing period. A phase-lock data-averaging procedure was subsequently performed over 90 rotor revolutions.

Numerical method

The numerical study presented in this paper was performed using the ANSYS CFX flow solver. The second stage of the turbine (Figure 4a) was meshed using a structured mesh with 8 million nodes, as shown in Figure 5b. The stator-rotor blade count ratio of the second stage is 3:4. As the periodicity is related to the stator-rotor blade count ratio, 30 deg were meshed. i.e. three stator passages and four rotor passages. The y^+ values on the walls were all below 30. The flow solver was run in unsteady mode using the transient rotor-stator interface. The results of the steady simulations were used as initial conditions. As a convergence criterion a reduction of the maximum mean square value for the residual from 10^{-2} to 10^{-6} was used. The standard k-ε turbulence model with a turbulence intensity of 5% at the inflow boundary layer was employed. The experimentally measured mass-averaged total pressure, together with the flow angle distribution and the static temperature constituted the boundary conditions at the inflow, whereas at the outflow the measured static pressure distribution was used for the steady simulation, which provided a good initial solution. The circumferential boundaries are periodic and a no-slip condition was applied at the adiabatic walls. Only the inlet cavity was simulated (Figure 5), introducing a leaking mass flow.

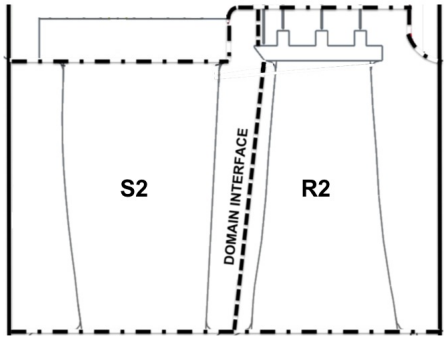

a.

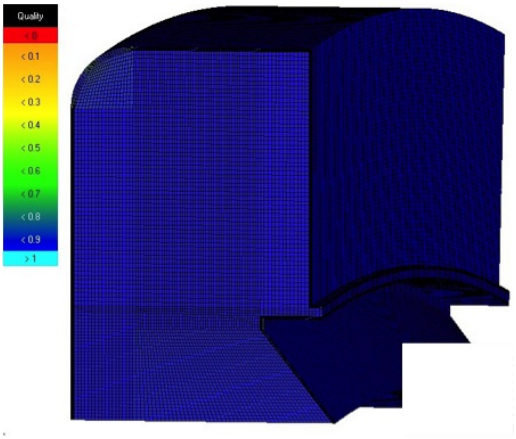

b.

Figure 5: a. The simulation domain is bordered by the measurement planes, solid lines at stage inlet and outlet. The center line sketches the simplified fluid path without the stator hub cavity. The domain interface is indicated by the dashed line. b. Mesh of the partial cavity

Validation

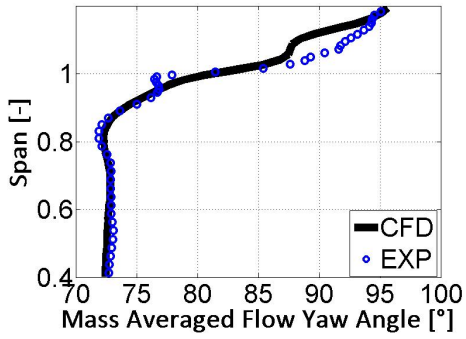

a.

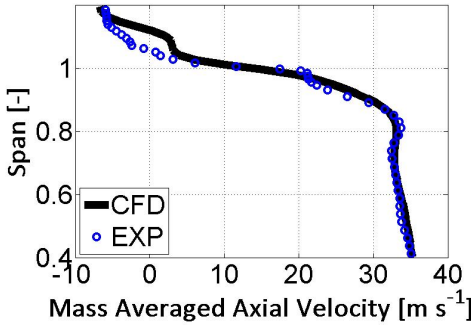

b.

Figure 6: Comparison of experiment and CFD for (a) the pitchwise mass-averaged flow yaw angle distribution and (b) the pitchwise mass-averaged axial velocity distribution at stator exit.

Figure 6 shows the comparison of experimental and numerical data for the pitchwise mass-averaged flow yaw angle and axial velocity distribution at stator exit. There is very good agreement within 0.5 degrees for the yaw angle up to 0.95 of the span. The CFD does not predict the underturning of the flow close to the upper casing. Moreover, inside the cavity, because of the strong secondary flows, the difference between experimental and computed results rise by up to 5 degrees. The pitchwise mass-averaged axial velocity shows a very good agreement over the blade span. The difference is within 1 m/s. Inside the cavity although the trend is captured, the CFD predicts higher velocities.

Results and discussion

In Figure 7, the experimentally measured flow relative yaw angle is shown against the rotor design blade metal angle at rotor inlet. The effect of the cavity flows is evident on the upper 20 percent of the blade span. Although the flow yaw angle follows the design angle till span 0.8, a large offset, increasing with span, is present from span 0.8 till 1.0. The mixing of the cavity and main flows results in the large positive yaw angle at the rotor blade reaching up to 40°-50° at the tip of the blade.

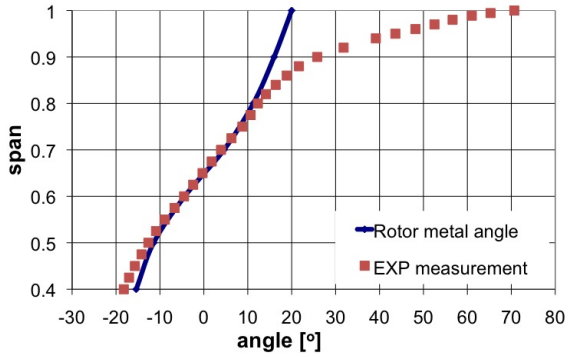

Figure 7: Metal angle of the 2nd rotor blade (blue line) and flow relative yaw angle experimentally measured at the inlet of the rotor (red dots)

The impact of the positive incidence on efficiency as compared to the other two cases, which were computationally studied, is presented in Figure 8. Design A, having a positive metal angle (+12 degrees) compared to the baseline case (-19 degrees), balances the large positive incidence of the baseline case. Therefore, an increase in efficiency 0.21% is calculated. On the other hand, the turning of the metal angle towards more negative values also led to an increase of 0.19% in efficiency. This is owing to the off-loading of the tip section. The camper angle of the blade is reduced, as are the losses because of the blade turning.

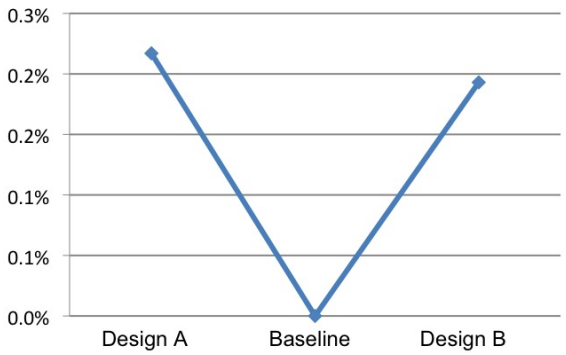

Figure 8: Total-to-total efficiency (computationally calculated) of the three cases compared in this study. The efficiency of the baseline case is used as reference.

As expected, the modification of the rotor leading edge towards more negative values results in a suction side flow diffusion, leading to an adverse pressure gradient, as shown in Figure 9, and a consequential flow separation. Contrary to Design B, Design A exhibits no suction side flow diffusion. The stagnation point has moved closer to the leading edge with the flow already being accelerated from the leading edge. The computations do not predict any influence of the leading edge modifications between the cases on the pressure side of the blade.

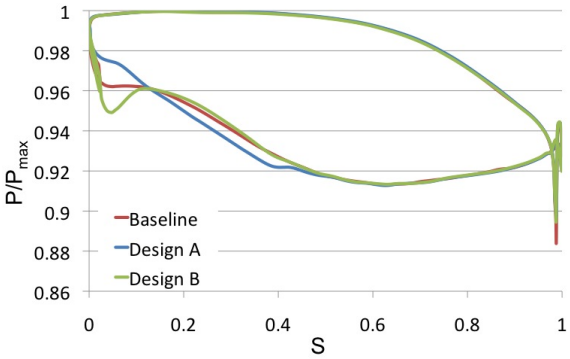

Figure 9: Blade loading of the cases examined at 95 percent of the blade span.

The formation of the corner vortex at the rotor blade for the three cases examined is shown in Figure 10 with a downstream view. The r-θ planes are colored to show radial velocity, with the red colored areas depicting upward-moving fluid, and transient averaged velocity vectors are projected on the planes. The two planes are axially distanced from the stator's trailing edge Z=0.968 and Z=1.126. The axial stator rotor distance at span=1.0 is used to non-dimensionalize. The backwards sweep of the leading edge of the baseline rotor causes the flow to migrate upwards in its vicinity, as shown in Figure 10a. Because of the positive incidence (Figure 7), the flow travels around the leading edge and over to the suction side. This results in the flow migrating in positive radial and circumferential directions. The merge with the flow from the blade suction side that moves under the negative flow yaw angle leads to the formation of a counterclockwise rotating vortex on the suction side close to the upper casing. Design A shows a reduced downward flow movement of the flow that is to travel around the blade, Figure 10c, as well as a less pronounced upward movement attached to the blade. As a result, although the vortex is formed at the same span location, it is profoundly weaker, leading to less mixing and hence producing less loss. Additionally, the counter-rotating vortex which was underneath the corner vortex in the baseline case is not present in the Design A case. On the other hand, as Design B has a leading edge design similar to the baseline case, the flow field is comparable with the one from the baseline case. Nevertheless, the intensity of the flow travelling over to the suction side is reduced. Moreover, the lean towards the suction side pushes the corner vortex to migrate at a lower span and lose strength. The small counter-rotating vortex underneath is now smaller.

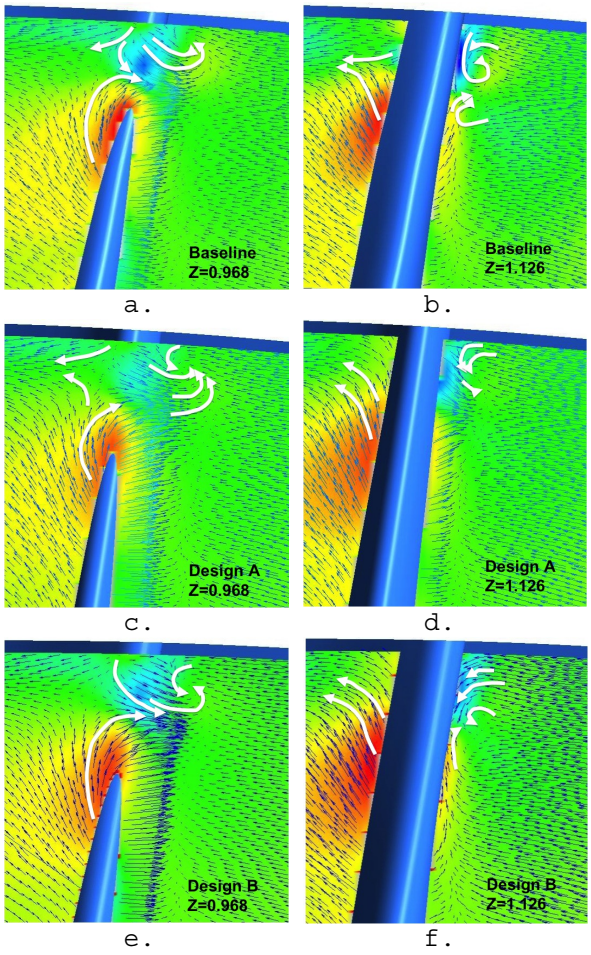

Figure 10: Downstream-looking r-θ planes at rotor inlet and for Z=0.968 (a, c and e) and Z=1.126 (b, d and f). The distance is non-dimensionalized with the stator-rotor distance at span 1.0. The planes are colored to show radial velocity and secondary flow vectors are projected onto the planes. The flow path is denoted with white lines.

In Figure 11, the radial mass flux into the cavity at cavity inlet (span 1.0) is shown for the three cases. The mass flux is axially summed and circumferentially plotted. Between the cases no measurable differences can be identified. Therefore, the leading edge geometry does not influence the oscillating cavity flow in and out of the cavity and hence the mixing process taking place. Nevertheless, it has to be mentioned that only the inlet cavity was modeled introducing a leakage flow that is constant for all cases.

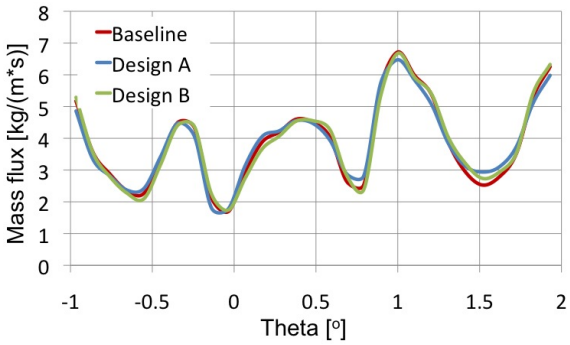

Figure 11: Radial mass flux into the cavity at cavity inlet (span 1.0) for all three cases examined in this study.

Conclusions

This paper examines the impact of geometrical modifications of the rotor leading edge geometry on stage efficiency. An initial experimental work was supplemented with computational analysis. Three different leading edge geometries have been studied.

The baseline leading edge was modified from an initial value of 19° compared to the axial direction to +12° for Design A and to -30° for Design B. Design A was intended to better match the flow conditions, namely the large positive incidence encountered by the rotor leading edge in the baseline case due to the influence of the cavity flows on the main flow. Design B was intended to examine the influence of off-loading the tip of the rotor blade.

Both modifications showed an efficiency increase relative to the baseline case. Although the leading edge modification had no measurable influence at the inlet cavity area, it did influence the flow around the leading edge, as well as the corner vortex formation on the suction side of the rotor blade. This resulted in an efficiency increase of 0.21% for Design A and 0.19% for Design B relative to the baseline case.

The corner vortex formed on the suction side of the rotor blade and close to the upper casing was noticeably reduced in Design A. The leading edge modification led to a weak crossing over of the fluid from the pressure to the suction side. Since the positive incidence was reduced, less mass flow traveled to the suction side, hence a weaker corner vortex was formed. The off-loading of the tip through the Design B modification also resulted in a weaker vortex, which migrated to a lower span location. Additionally, the modification created an adverse pressure gradient on the suction side.

Overall, this study suggests that the design of the rotor leading edge is not trivial. Slight modifications to the geometry cause the flow field around the blade to alternate, leading to efficiency increases.

References

1 Denton, J. D., 1993, "Loss Mechanisms in Turbomachines," The 1993 IGTI Scholar Lecture, ASME Journal of Turbomachinery, Vol. 115, pp. 621-656

2 Wallis, A. M., Denton, J. D. and Demargne A. A. J., 2001, "The Control of Shroud Leakage Flows to Reduce Aerodynamic Losses in a Low Aspect Ratio Shrouded Axial Flow Turbine," ASME Journal of Turbomachinery, Vol. 123, pp. 334-341

3 Rosic, B. and Denton, J. D., 2008, "Control of Shroud Leakage Loss by Reducing Circumferential Mixing," ASME Journal of Turbomachinery, Vol. 130, pp. 021010-1 – 021010-7

4 Mahle, I., 2010, "Improving the Interaction Between Leakage Flows and Main Flow in a Low Pressure Turbine," Proceedings of the ASME, paper No. GT2010-22448

5 Peters, P., Giboni, A., Menter, J. R., Pfost, H. and Wolter, K., 2005, "Unsteady Interaction of Labyrinth Seal Leakage Flow and Downstream Stator Flow in a Shrouded 1.5 Stage Axial Turbine," Proceedings of the ASME, paper No. GT2005-68065

6 Anker, J. E., Mayer, J. F. and Casey, M. V., 2005, "The Impact of Rotor Labyrinth Seal Leakage Flow on the Loss Generation in an Axial Turbine," Proceedings of the Institution of Mechanical Engineers, Part A: Journal of Power and Energy, Vol. 219, pp. 481-490

7 Gier, J., Stubert, B., Brouillet, B. and de Vito, L., 2005, "Interaction of Shrouded Leakage Flow and Main Flow in a Three-Stage LP Turbine," ASME Journal of Turbomachinery, Vol. 125, pp. 649-658

8 Pau, M., Cambuli, F. and Mandas, N., 2008, "Shroud Leakage Modeling of the Flow in a Two-Stage Axial Test Turbine," Proceedings of the ASME, paper No. GT2008-51093

9 Adami, P., Martelli, F. and Cecchi, C., 2007, "Analysis of the Shroud Leakage Flow and Main Flow Interactions in High-Pressure Turbines Using an Unsteady Computational Fluid Dynamics Approach," Proceedings of the Institution of Mechanical Engineers, Part A: Journal of Power and Energy, Vol. 221, pp. 837-848

10 Gregory-Smith, D. G., Ingram, G. and Jayaraman, P., Harvey, N. W. and Rose, M. G., 2001, "Non-Axisymmetric Turbine Endwall Profiling," Proceedings of the Institution of Mechanical Engineers, Part A: Journal of Power and Energy, Vol. 215, pp. 721-734

11 Sauer, H., Müller, R., and Vogeler, K., 2001, "Reduction of Secondary Flow Losses in Turbine Cascades by Leading Edge Modifications at the Endwall," ASME Journal of Turbomachinery, Vol. 123, pp. 207-213

12 Brenner, M. W., Sjolander, S. A. and Moustapha, S. H., 2003, "The Influence of Leading-Edge Geometry on Secondary Losses in a Turbine Cascade at the Design

Incidence," Proceedings of the ASME, paper No. GT2003-38107
13 Becz, S., Majewski, M. S. and Langston, L. S., 2003, "Leading Edge Modification Effects on Turbine Cascade Endwall Loss," Proceedings of the ASME, paper No. GT2003-38898
14 Perdichizzi, A. and Dossena, V., 1993, "Incidence Angle and Pitch-Chord Effects on Secondary Flows Downstream of a Turbine Cascade," ASME Journal of Turbomachinery, Vol. 115, pp. 383-391
15 Langston, L.S., 2001, "Secondary Flows In Axial Turbines – A Review," Annals of the New York Academy of Sciences, Vol. 934(1), pp. 11-26
16 Sieverding, C. H., 1985, "Recent Progress in the Understanding of Basic Aspects of Secondary Turbine Blade Passages," Journal of Engineering for Gas Turbines and Power, Vol. 107(2), pp. 248-257
17 Chaluvadi, V. S. P., Kalfas, I. A. and Hodson, H. P., 2003, "Vortex Transport and Blade Interactions in High Pressure Turbines," Proceedings of the ASME, paper No. GT2003-38389
18 Hodson, H. P. and Howell, R. J., 2005, "Bladerow Interactions, Transition, and High-Lift Aerofoils in Low-Pressure Turbines," Annual Review of Fluid Mechanics, Vol. 37, pp. 71-98
19 Schlienger, J., Kalfas, I. A. and Abhari, R. S., 2004, "Vortex-Wake-Blade Interaction in a Shrouded Axial Turbine," Proceedings of the ASME, paper No. GT2004-53915
20 Hodson, H. P. and Dawes, W. N., 1998, "On the Interpretation of Measured Profile Losses in Unsteady Wake-Turbine Blade Interaction Studies," ASME Journal of Turbomachinery, Vol. 120, pp. 276-284
21 Pfau, A., Schlienger, J., Rusch, D., Kalfas, I. A. and Abhari, R. S., 2003, "Unsteady Flow Interactions within the inlet Cavity of a Turbine Rotor Tip Labyrinth Seal," Proceedings of the ASME, paper No. GT2003-38271
22 Pfau, A., Kalfas, A. I. and Abhari, R. S., 2004, "Making use of Labyrinth Interaction Flow," Proceedings of the ASME, paper No. GT2004-53797
23 Schlienger, J., Pfau, A., Kalfas, A. I. and Abhari, R. S., 2003, "Effects of Labyrinth Seal Variation on Multistage Axial Turbine Flow," Proceedings of the ASME, paper No. GT2003-38270
24 Tashima, T., Sasaki, T., Kalfas, A. I. and Abhari, R. S., 2007, "Blade Loading Influence on Unsteady Flow Interactions in Axial Steam Turbines," Proceedings of the ASME, paper No. GT2007-27452
25 Pfau, A., Schlienger, J., Kalfas, A. I. and Abhari, R. S., 2003, "Unsteady, 3-Dimensional Flow Measurement Using a Miniature Virtual 4-sensor Fast Response Aerodynamic Probe (FRAP)," Proceedings of the ASME, paper No. GT2003-38128
26 Lenherr, C., Kalfas, A. I. and Abhari, R. S., 2007, "A Flow Adaptive Aerodynamic Probe Concept for Turbomachinery," Measurement Science and Technology Vol. 18, pp. 2599-2608